Chemical Engineering Journal 113 (2005) 41–46

Chemical Engineering Journal

www.elsevier.com/locate/cej

Selected oxide materials for sulfur removal

T. Zaki, M. Riad, L. Saad, S. Mikhail *

Egyptian Petroleum Research Institute, Nasr City, 11727 Cairo, Egypt

Received 21 February 2005; received in revised form 22 July 2005; accepted 23 August 2005

Abstract

The desulfurization activity of different selected oxide materials (iron, zinc, chromium, cobalt, and titanium oxides) blended with activated bentonite, in addition to nickel–tungsten/kaolinite catalysts, has been studied. The morphological and structural changes of the different materials were investigated via surface area, X-ray diffraction, and scanning electron microscope analyses. The desulfurization was carried out in an autoclave using dimethyl disulfide/cyclohexane solution as model compound.

The results indicate that the sorbent containing zinc–chromium–iron oxides is the most active one towards desulfurization, where DMDS removal reached ∼58% compared with the other prepared sorbents. This activity may be related to the ferromagnetic properties of both chromium and iron oxides.

Keywords: Desulfurization; Dimethyl disulfide; Iron; Zinc; Chrome

1. Introduction

Sulfur control in fuels is one of the most important problems for environmental protection, whereas the called zero sulfur fuels (below 10 ppm S) will be required in the future for the application of new exhaust gas cleaning technologies introduced by automobile manufacturers. In this connection, the terms “deep desulfurization” and “ultra-low sulfur fuels” have appeared in the literature recently [1–4].

Current gasoline desulfurization problem is dominated by the issues of sulfur removal from fcc naphtha, which contributes about 35% of gasoline pool but over 90% of sulfur in gasoline. Deep reduction of gasoline sulfur must be carried out without decreasing octane number or losing gasoline yield [5,6]. Approaches to reducing sulfur content in fcc naphtha include:

(1) post-treating product to remove sulfur from fcc naphtha;
(2) pre-treating the fcc feed to remove sulfur;
(3) increasing sulfur conversion in situ to hydrogen sulfide during the fcc operation.

The principles of the first method are based on one or more of the following processes: catalytic HDS, selective HDS, reactive adsorption using solid sorbent and hydrogen at elevated temperature and low hydrogen pressure, selective adsorption without using hydrogen at ambient temperature [5].

Because the favorable desulfurization activity of the different metal oxides, such as zinc, iron and cobalt, these oxides appear to be the most attractive towards desulfurization [7]. More recently using mixed oxides was found to improve the properties of single one. Mixed zinc oxide-hematite or zinc ferrite is a potential candidate for high temperature sulfur removal from reductive environment such as a coal-derived gas [8].

Tawara et al. [9] and Babich and Moulijn [10] studied the use of Ni/ZnO catalyst as sorbent for desulfurization of kerosene for fuel-cell applications, where nickel reacts with sulfur under hydrogen to form NiS, which consequently react with ZnO to form ZnS and regenerate nickel. Other authors used a mixture of zinc, copper, titanium and or cobalt oxides as tri-metal oxide catalysts [11,12].

The aim of the current work is to study the activity of different prepared mixed oxides: ZnO–Cr_2O_3–iron ore–bentonite, ZnO–TiO_2–iron ore–bentonite, ZnO–Cr_2O_3–$Co(OH)_2$–bentonite, ZnO–TiO_2–$Co(OH)_2$–bentonite, in addition to nickel–tungsten/kaolinite catalysts (having different concentration of tungsten ranging from 15 to 35 wt.%) to be used as adsorbents for desulfurization.

* Corresponding author. Fax: +20 2 2747433.
E-mail address: saramikhails@yahoo.com (S. Mikhail).

1385-8947/$ – see front matter © 2005 Elsevier B.V. All rights reserved.
doi:10.1016/j.cej.2005.08.004

Table 1
Chemical composition (wt.%) of the different four sorbents

Sample code	ZCF	ZTF	ZCCo	ZTCo
Fe_2O_3	40.9	40.9	1.9	1.9
ZnO	4.7	4.7	37.0	37.0
Cr_2O_3	3.1	–	24.6	–
TiO_2	0.8	3.9	0.6	25.2
CoO	–	–	8.4	8.4
SiO_2	24.4	24.4	17.7	17.7
Al_2O_3	6.7	6.7	4.9	4.9
CaO	5.0	5.0	–	–
MnO	2.3	2.3	–	–

2. Experimental

2.1. Samples preparation

The different prepared sorbents are included in Table 1. The different sorbents were prepared via mechanical mixing of different oxides with activated bentonite clay (from El-Hmamm district) for two hours. The raw bentonite clay was grounded and sieved to <125 μm and then subjected to acid activation [13].

The four sorbents: ZnO (BDH, assay >99%)–Cr_2O_3–iron ore–bentonite (ZCF), ZnO–TiO_2 (Merck)–iron ore–bentonite (ZTF), ZnO–Cr_2O_3–$Co(OH)_2$–bentonite (ZCCo), and ZnO–TiO_2–$Co(OH)_2$–bentonite (ZTCo) were calcined in a current of purified air for 12 h at 750 °C. Chromium oxide was precipitated from chromium chloride (Merck, assay >95%) by alkaline aqueous solution at ambient temperature; $Cr_2O_3{\cdot}nH_2O$ is formed as a green precipitate. The Egyptian iron ore supplied from "Upper Egypt" was grounded and sieved to <100 mesh. Cobaltous hydroxide is precipitated from cobaltous chloride (Merck, assay >99%) through the stepwise addition of ammonia solution.

Nickel–tungsten catalysts were prepared via impregnation technique using acid activated kaolinite as a support. The metals precursor were nickel chloride (Adwic, assay >97%) and ammonium tungstate (BDH), nickel was added with constant weight percentage "7", meanwhile the wieght percentage of tungsten is in the range from 15, 25 to 35. All such materials were dried and then calcined in purified air at 750 °C.

2.2. Structure and phase changes investigation

2.2.1. X-ray diffraction analysis

The X-ray diffraction patterns of the studied materials were recorded in the range $2\theta = 4$–70°, in a Brukur B_8 advance diffractometer with Cu $K\alpha_1$ radiation. The instrument was operated at 40 kV and the spectra were recorded at a scanning speed of 8°/min.

2.2.2. Nitrogen adsorption–desorption technique

The specific surface area (S_{BET}), total pore volume (V_p) and mean pore radius (r_H) of the different samples were measured using a Quantachrome NOVA-2000 Automated Gas Sorption System. Prior to such measurements all samples were perfectly degassed at 150 °C and evacuated at 10^{-4} Torr pressure for 3 h.

2.2.3. Scanning electron microscope

Morphology of sorbents and distribution of metallic species were revealed by scanning electron microscope (SEM) by using JEOL-JSM-6400 Microscope equipped with an energy dispersive X-ray analyzer. The images were taken with an emission current of 100 μÅ by a Wolframium filament and an accelerator voltage of 20 kV. The pretreatment of the samples consisted of coating with an evaporated gold film in a Balzers SCD004 sputter coater metallizator to increase the sorbents electric conductivity.

2.3. Evaluation of desulfurization activity

Five concentrations of dimethyl disulfide (DMDS) (Merck, assay >99%), in cyclohexane (EDWIC, assay >98%), were prepared namely: 0.08, 0.19, 0.26, 0.41 and 0.49 vol.%. No higher concentrations could be tested since the sulfur content in light petroleum fractions did not exceed 0.5 vol.%.

After drying the sorbent for two hours at 150 °C, desulfurization were carried out in a 500 mL mechanically stirred autoclave reactor (92-Rueil-Malmaison manufactured by Sotelem Co., USA) charged with 10 g of sorbent and 100 mL of dimethyl disulfide/cyclohexane solution at reaction temperature within the range 50–200 °C under a hydrogen pressure within 0.1–2.0 MPa.

The amount of sulfur compound removal was determined by analyzing the content of dimethyl disulfide before and after each experiment using high performance liquid chromatograph (HPLC), manufactured by WATERS, the chromatographic column was of type C18 reversed phase (250 mm × 4.6 mm). The UV detector (dual-wavelength UV of the type WATERS 2487) was adjusted at the wavelength of maximum adsorption, $\lambda_{max} = 254$ nm.

3. Results and discussion

3.1. Structure and phase changes investigation

3.1.1. X-ray diffraction analysis

Fig. 1 illustrates the X-ray diffraction pattern (XRD), which carried out to investigate the changes in the structure of the prepared zinc–chromium mixed oxides and to identify the new created crystalline phases after the insertion of iron ore.

For mixed activated bentonite–zinc–chromium oxides sorbent (ZC*), the X-ray diffraction pattern (Fig. 1a) shows that the detected bentonite lamella at *d*-spacing 14.46 Å completely disappeared upon the insertion of zinc–chromium oxides. This is due to the competition effect of the diffused ZnO and $2Cr^{3+}3O^{2-}$ (relatively bulk species) inside bentonite lamella, which permit the ZnO particles to insert inside bentonite lamella and not the chromium oxide particles as verified from the lines appearing at *d*-spacing 2.81, 2.60, and 2.47 Å characterize ZnO species (ASTM 89-0511).

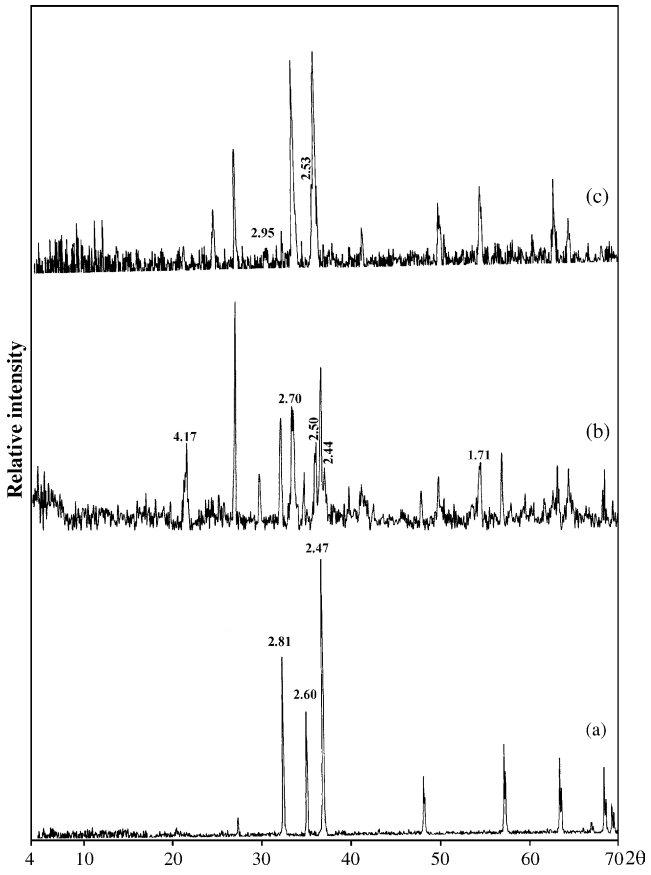

Fig. 1. X-ray diffraction patterns for (a) ZC*, (b) ZCF*, and (c) ZCF (asterisk (*) means uncalcined sorbent).

3.1.1.1. Effect of iron ore addition. For bentonite–zinc–chromium–iron ore mixed oxides sorbent ZCF*, X-ray diffraction pattern in Fig. 1b represent that after the addition of iron ore to the porous ZC* sorbent, the intensity of ZnO characteristic lines sharply decreased (it may be covered by iron ore phases). New lines appeared at *d*-spacing 2.70, 2.50 Å, which resulted from the presence of hematite Fe_2O_3 (ASTM 89-0598). Also, new lines appeared at *d*-spacing 4.17, 2.44, 1.71 Å, that is an indication for goethite FeO(OH) phase (ASTM 81-0464).

Upon calcination, the pattern of ZCF (Fig. 1c) shows the following:

- Complete disappearance of ZnO characteristic lines, this is due to the interaction of ZnO with iron or chromium oxides to form new oxide phases (zinc iron oxide $ZnFe_2O_4$, ASTM 01-1109) as indicated from the appearance of new lines at *d*-spacing 2.95 and 2.53 Å.
- Disappearance of goethite characteristics lines which indicates its conversion to Fe_2O_3 upon calcination. This is confirmed by the increase in intensity of hematite characteristic lines.

It is well known that as the atomic number increases the ionic radius increases, then on heating, the diffusion of metal species will be directed from chromium into iron then into ZnO. The active phase formed in between ZCF sorbent is a double phase of $ZnFe_2O_4$–Fe_2O_3. Also Cr_2O_3 is distributed into this active phase upon calcination.

Table 2
Calculated average crystallite size values for the prepared ZC and ZCF sorbents

2θ	Average crystallite size (nm)	
	ZC	ZCF
31.8	169.7	383.8
34.4	261.8	–
36.2	148.6	431.1

3.1.1.2. Crystallite size. Crystallite size for ZC and ZCF sorbents was determined according to Sherrer's equation at 2θ position: 31.8°, 34.4° and 36.2°. Data in Table 2 indicates that the crystallite size values show an increase upon the interaction of iron oxide with ZC sorbent after the calcination process. It increases from 169.7, and 148.6 nm (for ZC sorbent) to 383.8, and 431.1 nm, respectively (for ZCF sorbent). This increase is resulted from the interaction of iron oxide with ZC sorbent upon calcination and formation of iron mixed oxide phases that have larger crystallite size (in parallel with XRD data).

3.1.2. Nitrogen adsorption–desorption technique

Liquid nitrogen physisorption method was applied to the calcined prepared sorbents, to investigate the structural properties especially surface area. Data are presented in Table 3. The data revealed that, the surface area of ZC and ZT sorbents is nearly the same ~10.5 m^2/g.

For calcined tri-metal oxides (ZCF and ZTF) the surface area increased to reach 14.6 m^2/g as a result of the addition of iron ore to the previous di-metal oxides. This increase is accompanied with the formation of mixed iron oxide phases. On the other hand, the surface area of ZC slightly increased from 10.50 to 12.84 m^2/g upon the addition of cobalt oxide (sorbent ZCCo). This behavior can be explained by the fact that, Co_3O_4 [$CO^{2+}Co_2{}^{3+}O_4{}^{2-}$] is a bulky molecule, in addition, it has no magnetic properties compared with iron oxides species, consequently the formed mixed oxide phases may be aggregated and make agglomerate leading to a slight increase in ZC surface area upon the addition of cobalt oxide as compared to ZC and ZT upon the addition of iron ore. For ZTCo the measured

Table 3
Texural measurements of the prepared sorbents before and after calcination step

Sample code	S_{BET} (m^2/g)	V_p (mL/g)	r_H (Å)
Z	6.79	0.0056	16.49
ZC	10.43	0.0086	16.49
ZCF*	52.30	0.0415	15.87
ZCF	14.63	0.0116	15.86
ZCCo	12.84	0.0099	15.42
ZT	10.57	0.0090	17.03
ZTF	14.53	0.0114	15.69
ZTCo	8.75	0.0073	16.69
NiW35	6.26	0.0051	16.29

S_{BET} is the BET surface area, r_H the value of the average pore radius and V_p is the total pore volume (asterisk (*) means uncalcined sorbent).

surface area reached 8.75 m^2/g where it is lower than for ZT (10.5 m^2/g). This decrement, is due to the fact that: titanium (of TiO_2) present in rutile structure, which is stabilized by six-coordination oxygen atoms [14]. Thus, the tendency of titanium oxide species to attract and aggregate with the surrounded cobalt species increases. Consequently, the dispersion of particles and surface area decreases.

For nickel–tungsten sorbent, data in Table 3 clarifies that the surface area (6.5 m^2/g) is lower than that for the prepared calcined tri-metal oxide sorbent. This is an indication that the bulky crystallites of WO_3, which agglomerate together on calcination, leading to a decrease in particles dispersion, and also surface area.

To study the effect of calcination temperature on the surface area in the tri-metal oxides sorbents, N_2 adsorption measurements were carried out to zinc–chromium–iron oxides sorbent before calcination (ZCF*). It is clear that ZCF* sorbent has high surface area 52.34 m^2/g that is an indication for high dispersion of the small crystallites containing the sorbent. After calcination and formation of interacted oxide active phases, the crystallite size increased and the surface area decreased to 14.63 m^2/g (ZCF, Table 3). This is due to accumulation of iron oxide phases on the wall and around the pore mouth, resulting in a decrease in pore width. Thus, it can be concluded that calcination temperature serve in shrinkage and increase the amount of the shallower pore and considered to be a center for desulfurization [15].

3.2. Evaluation of desulfurization activity

Preliminary tests are carried out to investigate the extent of the adsorption of ZCF; the adsorption technique was carried out in batch reactor charged with 10 g of sorbent and 100 mL of 0.08, 0.19, 0.26, 0.41 and 0.49 vol.% dimethyl disulfide/cyclohexane solution at reaction temperature 50 °C for 2 h under a hydrogen pressure 0.5 MPa.

Fig. 2 represents the relation between the specific adsorption (adsorbed amount of mg adsorbate/g adsorbent) and the initial concentration of the adsorptive dimethyl disulfide in cyclohexane solution (mg DMDS/mL cyclohexane solution). From data, it is clear that, the adsorbed amount of dimethyl disulfide is found to increase linearly with the gradual increase in the concentration of dimethyl disulfide in cyclohexane solution from 0.87 to 5.19 mg DMDS/mL cyclohexane solution, i.e., the specific adsorption (adsorbed amount of mg adsorbate/g adsorbent) increased gradually with the increase in the concentration of the adsorbate.

Accordingly, the adsorptive power of the different prepared sorbents towards dimethyl disulfide desulfurization were studied in batch reactor charged with 10 g of sorbent and 100 mL of the highest concentration of dimethyl disulfide/cyclohexane solution (0.49 vol.%) at reactor temperature range within 50–200 °C under a hydrogen pressure 0.5 MPa. The effect of reaction temperature on DMDS adsorption for the four sorbents ZCF, ZTF, ZCCo, and ZTCo are illustrated in Fig. 3.

Zinc–chromium–iron oxides sorbent (ZCF) was found to be the most active adsorbent, whereas the DMDS removal percentage increased from 10.10 to 58.14 by raising the temperature

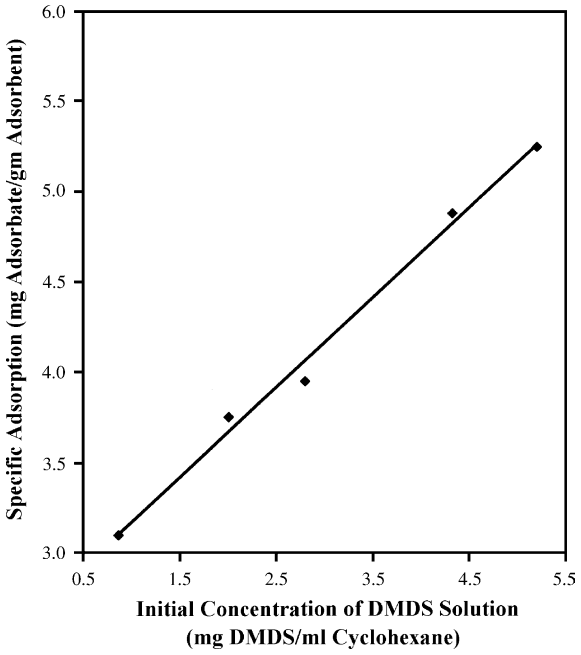

Fig. 2. Relation between specific adsorption and initial concentration of DMDS for ZCF sorbent.

from 50 to 200 °C successively. This may be due to the fact that both zinc and iron oxides are capable of reacting with sulfide compounds at high temperatures, in spite of the fact that the thermodynamics for Fe_2O_3–S are less favorable than for the ZnO–S reaction [16]. In addition to that, the presence of chromium oxide, which has the ability to sulfided (Cr-sulfide and/or Cr-oxysulfide) [17], may be considered as important parameter for such high activity for ZCF sorbent. On the other hand, ZTF sorbent showed comparable data with respect to ZCF one, in temperature range of 50 and 150 °C, such adsorption power may due to the relatively easiness for titania sulfidation [18].

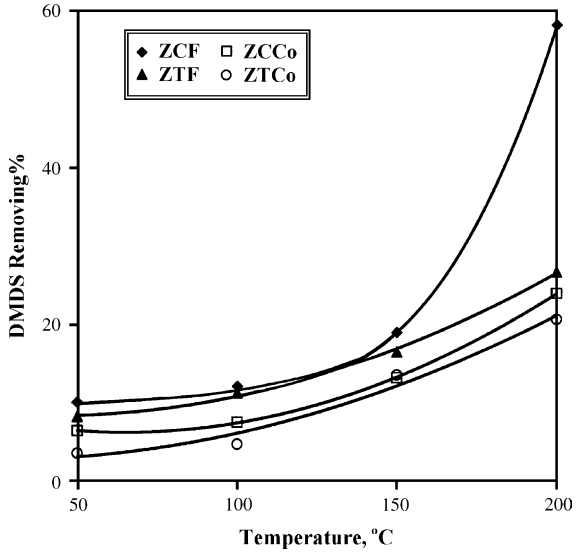

Fig. 3. Effect of reaction temperature on DMDS adsorption for ZCF, ZTF, ZCCo, and ZTCo sorbents.

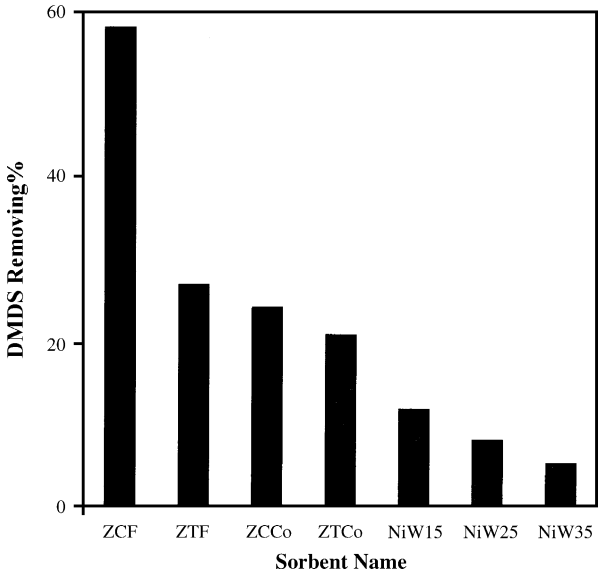

Fig. 4. Relation between adsorption of DMDS and type of sorbent at reaction temperature 200 °C.

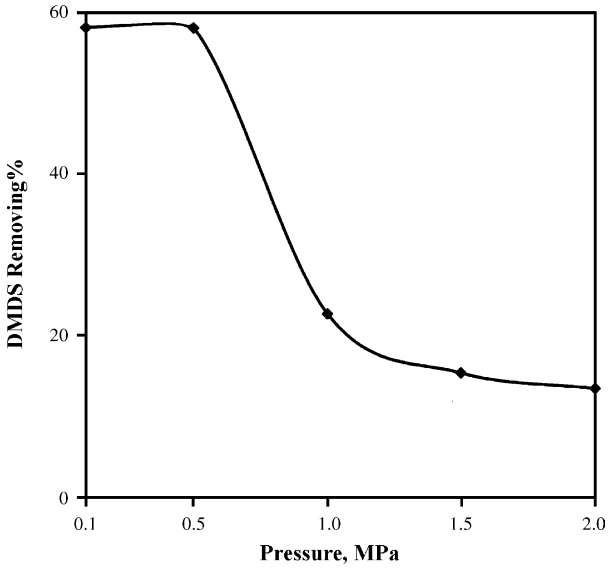

Fig. 5. Effect of hydrogen pressure on DMDS adsorption for ZCF sorbent.

The sorbent ZCCo demonstrates activity less than the previous sorbents, "ZCF, and ZTF", this may be due to that the reactant formed a dense film surrounding the sorbent and prevents further entrance of reactant inside the bulk sorbent (ZCCo); accordingly, this sorbent shows a lower activity for desulfurization.

Fig. 4 shows a comparison between the adsorptive power of the previous samples and the conventional tungsten–nickel oxides/kaolinite samples (NiW15, NiW25, and NiW35), at reaction temperature 200 °C. The histogram clarify decreasing in the adsorption activity in the following manner: ZCF > ZTF > ZCCo > ZTCo > NiW15 > NiW25 > NiW35. The ordering of the adsorption activities of the tested samples proportionate with their surface area values (Table 3).

On the other hand, the decrease in adsorption efficiency of Ni–W/kaolinite with the increase in tungsten oxide content is in agreement with Bendezú et al. observation [19], whereas the bulky crystallites of WO_3 that agglomerate together on calcination, leading to a decrease in nickel oxide dispersion, and so making its efficiency towards desulfurization more difficult.

According to the previous findings, the influence of hydrogen pressure on the most active ZCF sorbent was studied at reaction temperature 200 °C and using dimethyl disulfide/cyclohexane solution of concentration 0.49 vol.%. The experimented hydrogen pressures ranged from 0.1 to 2.0 MPa, since, according to the industry requirements, reaction temperatures and pressures below 450 °C and 3.5 MPa, respectively, are desirable, hence, as the process operates at lower pressure, as the hydrogen or olefins does not consume [5,20,21].

Fig. 5 elucidates that, the adsorption power of ZCF sorbent is not affected by variation in hydrogen pressure from 0.1 to 0.5 MPa where the DMDS removal percentage was approximately 58%. By raising the pressure to 1.0 MPa the removal percentage decreased to 22.75%. The decrease in the sorbent activity by increasing the reaction pressure continued until DMDS removal percentage reaches 13.48% at hydrogen pressure 2.0 MPa.

It was found that the high adsorption efficiency of the sorbent ZCF towards DMDS removal is mainly due to the high activity of zinc and/or iron metals containing sorbent, which react with sulfur atom to form metal sulfide as verified from X-ray diffraction pattern for ZCF after desulfurization (Fig. 6). X-ray diffraction pattern showed the appearance of different new lines at *d*-spacing 2.62, 2.04, 1.69 and 3.33, 2.94, 1.92 Å, which are indications for the formation of chromium and zinc sulfides, respectively (ASTM 11-0007 and ASTM 75-1547 successively). Also, new lines reveals the presence of different iron sulfide phases are appeared at *d*-spacing 2.98, 2.51, 1.75 Å (ASTM 23-1122) and 2.98, 2.69, 2.10 Å (ASTM 02-1204). The creation of such sulfides is indication for the destroying of zinc ferrite phase to zinc oxide and hematite, which then converted to the corresponding

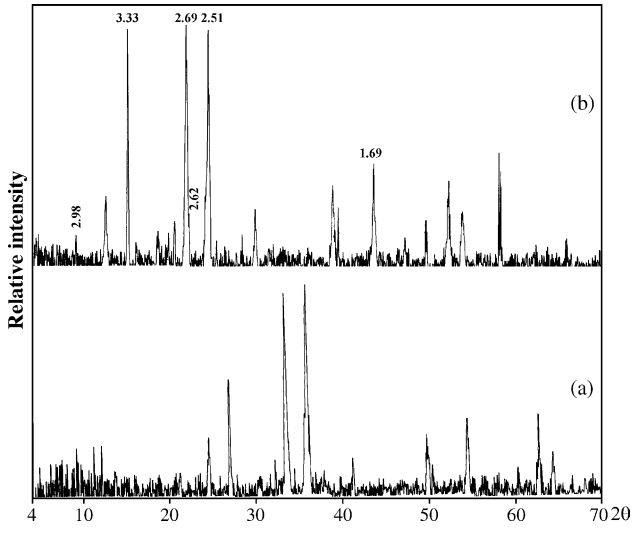

Fig. 6. X-ray diffraction pattern for ZCF sorbent (a) before and (b) after desulfurization.

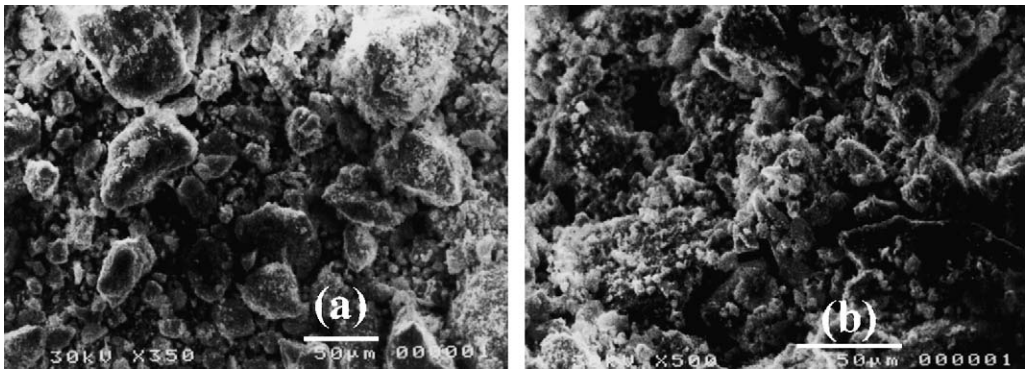

Fig. 7. Scanning electron microscope photomicrograph for ZCF sorbent (a) before and (b) after desulfurization.

sulfide, forms ZnS and FeS, respectively, upon the desulfurization [12].

SEM was used to obtain the morphology of ZCF before and after desulfurization. The morphology of ZCF sorbent in Fig. 7a appears to be constituted of irregular hexagonal crystallites of various sizes that are non-homogeneously distributed. Some bulky agglomerates actually result from the growth of particles with high surface energy such as ZnO and Fe_2O_3, which may interact to form spinel-phase $ZnFe_2O_4$ as confirmed by X-ray diffractogram. This is in accordance also with the observed decrease in the surface area accompanying the calcination process as well as the observed increase in crystallite size. However, the non-homogeneous distribution of various particles with various sizes may be also attributed to the formation of $ZnFe_2O_4$ spinel structure as well as the dispersion of the tiny chromium oxide particles in-between.

SEM picture for the used ZCF sorbent as represented in Fig. 7b indicates that after desulfurization; the crystallites size seemed to be diminished due to the formation of smaller crystallites of metal sulfide compared with the bulky spinel crystallites. Therefore, the observation of population of smaller particles is not due to sintering process but rather to the fact that a major proportion of metal oxide species are being sulfided through the reaction that occurred between sulfur containing compounds in the feedstock and the metal species in the sorbent. The sulfided metal particles are appeared to aggregate and stacking in disordered manner. This is evidenced due to the fact that desulfurization cause the gathering of the metal sulfide species, which aggregate and re-crystallize giving rise to a continuous layer FeS and ZnS on the external surface of the sorbent and consequently the desulfurized product obtained, contains less sulfur content.

In addition, The physico-chemical properties of the ZCF sorbent has essential effect in its activity towards desulfurization, in such a manner that ZCF is rich with different electron deficient metals which acting as active sites for desulfurization and these metals are contributed in different crystalline oxide phases as estimated from XRD patterns. Also, the iron metal acts as trigger substance for carbon deposition, which is harmful to the desulfurization performance. The sorbent is characterized by moderate crystallite size, which allows high dispersion and consequently high surface area. In addition, the sorbent is rich with moderate pores suitable for desulfurization as confirmed from nitrogen adsorption–desorption measurements.

4. Conclusion

In summarizing the results shown above, the following conclusions can be deduced:

- A zinc–chromium–iron oxides sorbent (ZCF) is the most active one within the different adsorbents, whereas the DMDS removal percentage reached 58.14 by raising the temperature to 200 °C.

References

[1] M. Yumoto, K. Usui, K. Watanabe, K. Idei, H. Yamazaki, Catal. Today 35 (1997) 45.
[2] M.V. Landau, Catal. Today 36 (1997) 393.
[3] E. Pedernera, R. Reimert, N. Luan Nguyen, V. van Buren, Catal. Today 79/80 (2003) 371.
[4] M. Zdražil, Catal. Today 86 (2003) 151.
[5] C. Song, Catal. Today 86 (2003) 211.
[6] X. Ma, L. Sun, C. Song, Catal. Today 77 (2002) 107.
[7] E. Sasaoka, K. Taniguchi, M.A. Uddin, S. Kasaoka, Y. Sakata, Energy Fuels 8 (1994) 1100.
[8] E. Sasaoka, Y. Iwamoto, M.A. Uddin, Y. Sakata, Energy Fuels 9 (1995) 344.
[9] K. Tawara, T. Nishimura, H. Iwanami, T. Nishimoto, T. Hasuike, Ind. Eng. Chem. Res. 40 (2001) 2367.
[10] I.V. Babich, J.A. Moulijn, Fuel 82 (2003) 607.
[11] E. Sasaoka, N. Sada, A. Manabe, M.A. Uddin, Y. Sakata, Ind. Eng. Chem. Res. 38 (1999) 958.
[12] H.K. Jun, T.J. Lee, J.C. Kim, Ind. Eng. Chem. Res. 41 (2002) 4733.
[13] S. Mikhail, N. Rizk, I.K. Abdou, Revue de L'institut Français du Pétrole XXVI (1971) 1213.
[14] A.F. Wells, Structural Inorganic Chemistry, 4th ed., Oxford University Press, Oxford, 1975.
[15] M. Kobayashi, H. Shiria, M. Vunokawa, Energy Fuels 11 (1997) 887.
[16] J.D. White, F.R. Groves Jr., D.P. Harrison, Catal. Today 40 (1998) 47.
[17] M. Sychev, V.H.J. San de Beer, A. Kodentsov, E.M. van Oers, R.A. van Santen, J. Catal. 168 (1997) 245.
[18] Z.B. Wei, W. Yan, H. Zhang, T. Ren, Q. Xin, Z. Li, Appl. Catal. A 167 (1998) 39.
[19] S. Bendezú, R. Cid, J.L.G. Fierro, A. López Agudo, Appl. Catal. A 197 (2000) 47.
[20] C. Pophal, F. Kameda, K. Hoshino, S. Yoshinaka, K. Segawa, Catal. Today 39 (1997) 21.
[21] C. Song, X. Ma, Appl. Catal. B 41 (2003) 207.